Single-atomic cobalt sites embedded in hierarchically ordered porous nitrogen-doped carbon as a superior bifunctional electrocatalyst

Tingting Sun[a,1], Shu Zhao[b,1], Wenxing Chen[a,1], Dong Zhai[c,d], Juncai Dong[e], Yu Wang[f,2], Shaolong Zhang[a], Aijuan Han[a], Lin Gu[g], Rong Yu[h], Xiaodong Wen[i], Hanlin Ren[a], Lianbin Xu[j], Chen Chen[a], Qing Peng[a], Dingsheng Wang[a,2], and Yadong Li[a,2]

[a]Department of Chemistry, Tsinghua University, Beijing 100084, China; [b]Beijing Guyue New Materials Research Institute, Beijing University of Technology, Beijing 100124, China; [c]Materials Genome Institute, Shanghai University, Shanghai 200444, China; [d]Department of Physics, International Centre for Quantum and Molecular Structures, Shanghai University, Shanghai 200444, China; [e]Beijing Synchrotron Radiation Facility, Institute of High Energy Physics, Chinese Academy of Sciences, Beijing 100049, China; [f]Shanghai Synchrontron Radiation Facility, Shanghai Institute of Applied Physics, Chinese Academy of Science, Shanghai 201800, China; [g]Beijing National Laboratory for Condensed Matter Physics, Institute of Physics, Chinese Academy of Sciences, Beijing 100190, China; [h]Beijing National Center for Electron Microscopy, School of Materials Science and Engineering, Tsinghua University, Beijing 100084, China; [i]State Key Laboratory of Coal Conversion, Institute of Coal Chemistry, Chinese Academy of Sciences, Taiyuan 030001, China; and [j]State Key Laboratory of Organic–Inorganic Composites, Beijing University of Chemical Technology, Beijing 100029, China

Edited by Alexis T. Bell, University of California, Berkeley, CA, and approved November 1, 2018 (received for review August 7, 2018)

Exploring efficient and cost-effective catalysts to replace precious metal catalysts, such as Pt, for electrocatalytic oxygen reduction reaction (ORR) and hydrogen evolution reaction (HER) holds great promise for renewable energy technologies. Herein, we prepare a type of Co catalyst with single-atomic Co sites embedded in hierarchically ordered porous *N*-doped carbon (Co-SAS/HOPNC) through a facile dual-template cooperative pyrolysis approach. The desirable combination of highly dispersed isolated atomic Co-N_4 active sites, large surface area, high porosity, and good conductivity gives rise to an excellent catalytic performance. The catalyst exhibits outstanding performance for ORR in alkaline medium with a half-wave potential ($E_{1/2}$) of 0.892 V, which is 53 mV more positive than that of Pt/C, as well as a high tolerance of methanol and great stability. The catalyst also shows a remarkable catalytic performance for HER with distinctly high turnover frequencies of 0.41 and 3.8 s^{-1} at an overpotential of 100 and 200 mV, respectively, together with a long-term durability in acidic condition. Experiments and density functional theory (DFT) calculations reveal that the atomically isolated single Co sites and the structural advantages of the unique 3D hierarchical porous architecture synergistically contribute to the high catalytic activity.

single-atomic cobalt sites | oxygen reduction reaction | hydrogen evolution reaction | in situ XAS measurements | hierarchically ordered porous structure

Electrocatalytic oxygen reduction reaction (ORR) and hydrogen evolution reaction (HER) are two key constituent parts of fuel cells, water splitting, and metal-air batteries (1–3). Efficient electrocatalysts are critically important to improve ORR and HER efficiencies by promoting the reaction kinetics (4–6). Although precious-metal (e.g., Pt)-based catalysts are currently identified as the excellent electrocatalysts in catalyzing ORR and HER, their poor abundance and high cost significantly restrict their large-scale application (7, 8). Recently, transition-metal (Fe, Co, Ni, Mo, and W)-based catalysts have been widely studied as potential substitutes because of their promising catalytic properties (9–11). In an effort to achieve enhanced catalytic performances of these catalysts, one common strategy is to downsize the catalysts to nanoscale to engender more exposed active sites (12).

Single-atomic-site (SAS) catalysts, which represent the ultimate small-size limit to obtain the maximum atom utilization and expose the most active sites, have recently attracted great attention in heterogeneous catalysis (13–17). However, it remains a significant challenge to synthesize SAS catalysts together with accurate control of the microstructures because the single-metal atoms with high surface free energy are easy to bring about aggregation and migration (18, 19). As is well-known, anchoring single-metal atoms on a supporting substrate through the strong interaction between metal and its substrate provides an effective way for stabilizing these single atoms (20–23). A crucial component in the design of the supporting material for electrocatalysis is the specific surface area and porous structure, which determines the transport of reactants and products and the accessible part of active sites (24–27). Although metal single-atom catalysts with various porous structure have been constructed to further enhance the catalytic properties, accurate control of the ordering and homogeneity of the pores in multiscales has not been achieved, which possibly still restricts the mass diffusion in the electrode and then limits the catalytic process on the active moieties.

To obtain SAS catalysts with highly dispersed catalytic sites, ordered hierarchical pore structure, and high conductivity,

Significance

A crucial component in the design of the single-atomic-site (SAS) catalysts for electrochemical applications is the specific surface area and porous structure. Here, we synthesize a type of Co catalyst with single-atomic Co sites embedded in hierarchically ordered porous *N*-doped carbon showing superior bifunctional activity for oxygen reduction reaction and hydrogen evolution reactions. Combined control experiments, density functional theory calculations, and in situ X-ray absorption spectroscopy measurements uncover that the atomically isolated Co-N_4 coordination and the unique 3D porous open architecture synergistically contribute to the excellent catalytic performance. The dual-template-assisted strategy sheds insight on the construction of structurally controllable SAS catalysts for various applications, and the investigation of enhancement mechanism provides great help to boost the efficiency of future cost-effective electrocatalysts.

Author contributions: D.W. and Y.L. designed research; T.S. performed research; T.S., S. Zhao, W.C., D.Z., J.D., Y.W., S. Zhang, A.H., L.G., R.Y., X.W., H.R., L.X., C.C., and Q.P. analyzed data; and T.S. and D.W. wrote the paper.

The authors declare no conflict of interest.

This article is a PNAS Direct Submission.

[1]T.S., S. Zhao, and W.C. contributed equally to this work.

[2]To whom correspondence may be addressed. Email: wangyu@sinap.ac.cn, wangdingsheng@mail.tsinghua.edu.cn, or ydli@mail.tsinghua.edu.cn.

This article contains supporting information online at www.pnas.org/lookup/suppl/doi:10.1073/pnas.1813605115/-/DCSupplemental.

Published online November 28, 2018.

herein, we first synthesize single-atomic Co sites embedded in hierarchically ordered porous *N*-doped carbon (Co-SAS/HOPNC) via a facile dual-template cooperative pyrolysis strategy. This material offers the desirable combination of abundant atomically isolated Co-N species as active sites for catalytic reactions, high surface area from the mesopores for affording sufficient active site exposure, and hierarchically ordered interconnected macro/mesoporous structure for shortening molecule/ion diffusion length in the electrolyte and maximizing the mass/charge diffusion throughout the electrode and thus significantly enhancing the accessibility to the active sites, giving rise to an excellent bifunctional electrocatalytic performance for ORR and HER. The Co-SAS/HOPNC exhibits a high half-wave potential ($E_{1/2}$) of 0.892 V for ORR in 0.1 M KOH, as well as high turnover frequencies (TOFs) of 0.41 and 3.8 s^{-1} at an overpotential of 100 and 200 mV, respectively, for HER in 0.5 M H_2SO_4. In addition, this catalyst shows a high durability for these two reactions. Experiments and density functional theory (DFT) calculations reveal that the atomically dispersed isolated Co-N_4 sites in porous carbon contribute greatly to the remarkable catalytic performance. The present synthetic method could also allow access to other M-SAS/HOPNC materials (M = Fe, Ni, etc.), which may offer new opportunities for SAS catalysts in various applications.

Results and Discussion

Synthesis and Characterization of the Co-SAS/HOPNC Catalyst. The fabrication procedure for the Co-SAS/HOPNC is described in Fig. 1*A*. Silica colloidal crystal (opal) and triblock copolymer Pluronic F127 were used as macroporous mold and mesostructural template, respectively. A precursor solution containing resol (carbon source), dicyandiamide, vitamin B12 (VB12), and F127 was first infiltrated into the void space of the silica opal; then, the mesostructure was formed during an evaporation induced self-assembly (EISA) process. Subsequent pyrolysis and then removal of the silica opal template yielded freestanding Co-SAS/HOPNC (preparation details are provided in *SI Appendix*). The SEM images (Fig. 1*B* and *SI Appendix*, Fig. S1) show that Co-SAS/HOPNC has an ordered 3D-interconnected macroporous architecture with open windows between adjacent spherical voids. From the transmission electron microscopy (TEM) image of Co-SAS/HOPNC (Fig. 1*C*), uniform macropores and well-defined mesopores located in the macropore walls can be observed. The N_2 adsorption–desorption isotherms indicate the presence of a mesoporous structure in the Co-SAS/HOPNC with a high Brunauer–Emmett–Teller surface area of 716 m^2 g^{-1} and a total pore volume of 1.78 cm^3 g^{-1} (Fig. 1*D*). In addition, a distribution of pores concentrated at around 10.8 nm can be observed from Fig. 1*D* (*Inset*). The high porosity of the Co-SAS/HOPNC is important for providing sufficient space for facile diffusion of reactants and product molecules to and from the confined Co sites, giving rise to favorable catalytic kinetics (28–31). Energy-dispersive X-ray spectroscopy (EDS) analysis in an scanning transmission electron microscope (SEM) (Fig. 1*E*) confirms the existence of Co, N, and C elements throughout the ordered porous structure. The isolated single Co atoms dispersed on the *N*-doped porous carbon matrix can be identified in the aberration-corrected high-angle annular dark-field SEM (AC HAADF-STEM) image (Fig. 1 *F* and *G*). Bright dots marked by light-yellow cycles correspond to individual Co atoms. The ring-like selected area electron diffraction pattern (*SI Appendix*, Fig. S2*A*) indicates the poor crystallinity of the Co-SAS/HOPNC, in agreement with the powder X-ray diffraction analysis (*SI Appendix*, Fig. S2*B*). Inductively coupled plasma–atomic emission spectrometry analysis demonstrated that the Co content in the Co-SAS/HOPNC catalyst was about 0.49 wt % (*SI Appendix*, Table S1). X-ray photoelectron spectroscopy analysis was performed to investigate the binding states of C and N in the Co-SAS/HOPNC (*SI Appendix*, Fig. S3). The N1s spectrum of Co-SAS/HOPNC reveals that four types of nitrogen coexist, including pyridinic N (398.8 eV),

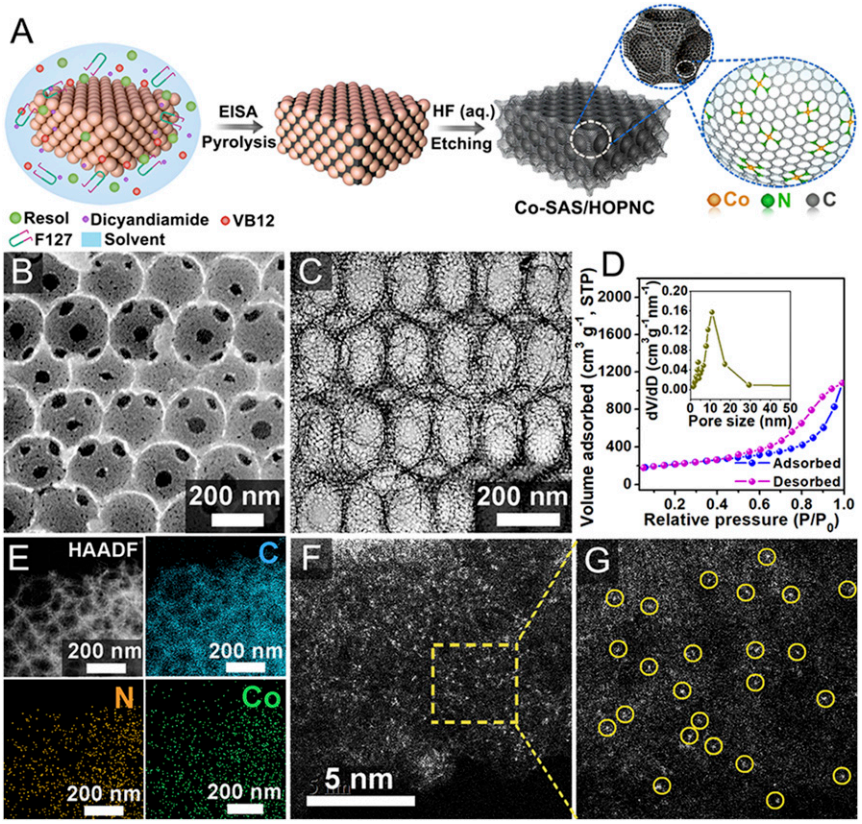

Fig. 1. Synthesis and characterization of Co-SAS/HOPNC catalyst. (*A*) Schematic illustration of the preparation of Co-SAS/HOPNC. (*B*) SEM and (*C*) TEM image of Co-SAS/HOPNC. (*D*) N_2 adsorption–desorption isotherms of Co-SAS/HOPNC. (*Inset*) Pore-size distribution curve. (*E*) HAADF-STEM image and corresponding EDS maps of Co-SAS/HOPNC. (*F* and *G*) AC HAADF-STEM images of the Co-SAS/HOPNC. Isolated single Co atoms are marked with light-yellow circles.

pyrrolic N (399.7 eV), graphitic N (401.1 eV), and oxidized-N (404.6 eV).

X-ray absorption near-edge structure (XANES) and extended X-ray absorption fine structure (EXAFS) spectroscopies were used to further probe the structure of Co species at the atomic level. Fig. 2*A* shows the Co *K*-edge XANES spectra of Co-SAS/HOPNC and several references, including Co foil, CoO, and Co_3O_4. The position of absorption edge for Co-SAS/HOPNC implies that the valence of Co atom is situated between Co^0 and Co^{2+}. The Fourier-transformed (FT) k^3-weighted EXAFS profile at Co edge for Co-SAS/HOPNC (Fig. 2*B*) only displays one strong peak around 1.32 Å, which is mainly ascribed to the Co-N/C coordination at the first shell. Also, the Co–Co interaction peak at 2.17 Å or other high-shell peaks are absent. These results suggest that the Co atoms are atomically dispersed in Co-SAS/HOPNC, which is consistent with the AC HAADF-STEM observation. Wavelet transform (WT) of Co *K*-edge EXAFS analysis was carried out to further demonstrate the atomic dispersion of Co in Co-SAS/HOPNC (Fig. 2*C*). As shown in the WT contour plots of the Co-SAS/HOPNC, only one intensity maximum at 4 $Å^{-1}$ is detected and can correspond to the Co-N(C) coordination. In addition, no intensity maximum belonging to Co–Co contribution can be observed, in contrast with the WT plots of Co foil, CoO, and Co_3O_4. The quantitative structural parameters of Co atoms in Co-SAS/HOPNC were extracted by conducting the EXAFS fitting. The fitting curves are shown in Fig. 2 *D* and *E* and the fitting parameters are summarized in *SI Appendix*, Table S2. The fitted coordination number of the central Co atom in the first shell is around 4 at a distance of 1.96 Å (Fig. 2*E*, *Inset*). This result indicates that in Co-SAS/HOPNC the Co is atomically distributed in the *N*-doped hierarchically porous carbon matrix and coordinated by four N atoms. The best-fit results of Co foil are given in *SI Appendix*, Fig. S4 for comparison.

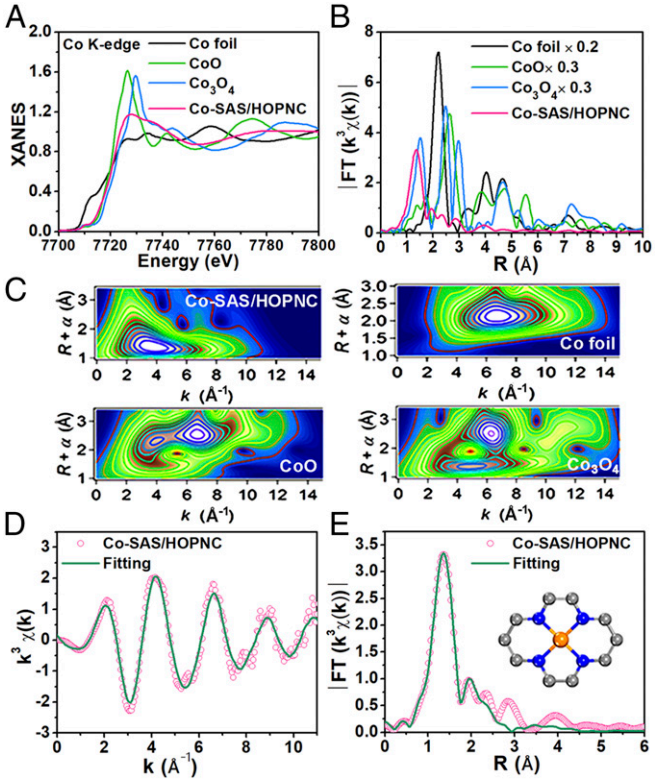

Fig. 2. Structural analysis of Co-SAS/HOPNC. (*A*) XANES spectra and (*B*) FT-EXAFS curves of Co-SAS/HOPNC, CoO, Co_3O_4, and Co foil at Co *K* edge. (*C*) WT-EXAFS of Co-SAS/HOPNC, Co foil, CoO, and Co_3O_4. (*D*) The corresponding EXAFS fitting curves of Co-SAS/HOPNC at *k* space. (*E*) The corresponding EXAFS fitting curves of Co-SAS/HOPNC at *r* space. (*Inset*) Schematic model of Co-SAS/HOPNC: Co (orange), N (blue), and C (gray).

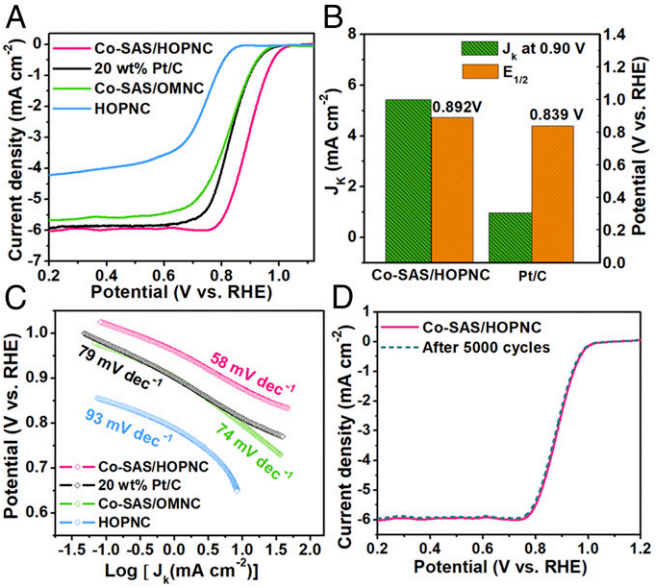

Fig. 3. Electrocatalytic performance evaluation of catalysts for ORR in O_2-saturated 0.1 M KOH. (*A*) ORR LSV curves for different catalysts at the rotating rate of 1,600 rpm (scan rate: 5 mV s^{-1}). (*B*) J_k at 0.90 V and $E_{1/2}$ for various samples. (*C*) Tafel slopes of different catalysts derived from the LSV curves. (*D*) ORR LSV curves of Co-SAS/HOPNC initially and after 5,000 cycles between 0.5 and 1.0 V at a scan rate of 100 mV s^{-1}.

Electrocatalytic Performance Evaluation for ORR. The ORR electrocatalytic activity of the Co-SAS/HOPNC catalyst was examined in O_2-purged 0.1 M KOH by using rotating disk electrode measurements. The catalytic activities of the HOPNC (*SI Appendix*, Fig. S5), ordered macroporous *N*-doped carbon with single atomic Co sites (Co-SAS/OMNC, *SI Appendix*, Figs. S6 and S7), and commercial 20 wt % Pt/C were also studied under the identical condition for comparison. The linear sweep voltammogram (LSV) curves shown in Fig. 3*A* reveal that the Co-SAS/HOPNC catalyst has a high ORR activity among the studied catalysts in view of the most positive onset (E_{onset}) and half-wave ($E_{1/2}$) potentials. The $E_{1/2}$ of Co-SAS/HOPNC (0.892 V) was 53 mV more positive than that of Pt/C, as well as better than that of most ORR electrocatalysts based on non-precious-metal materials (*SI Appendix*, Table S3). The Co-SAS/HOPNC catalyst also shows outstanding ORR activity under acidic electrolyte (*SI Appendix*, Fig. S8). These results confirm the significance of the formation of Co-N_4 active sites and hierarchical porous structure for boosting ORR activity. LSV tests under various rotation speeds (400–2,500 rpm) were conducted to probe the catalytic kinetics (*SI Appendix*, Fig. S9*A*). The corresponding Koutecky–Levich (K–L) plots at different potentials present good linearity with similar slopes (*SI Appendix*, Fig. S9*B*), which indicates first-order reaction kinetics toward the oxygen concentration (32). On the basis of the K–L equation, an electron transfer number (*n*) of 3.9 was yielded for Co-SAS/HOPNC, which approaches the theoretical value of Pt/C (4.0, *SI Appendix*, Fig. S10), revealing that the oxygen reduction process on the isolated Co sites proceeds through a near-four-electron pathway with excellent selectivity of direct O_2 reduction to OH^-. Moreover, the kinetic current density (J_k) at 0.90 V vs. reversible hydrogen electrode for Co-SAS/HOPNC electrode (5.42 mA cm^{-2}) is about 5.6 times that of Pt/C (0.96 mA cm^{-2}) (Fig. 3*B*), demonstrating the superior ORR activity of the Co-SAS/HOPNC catalyst. As shown in

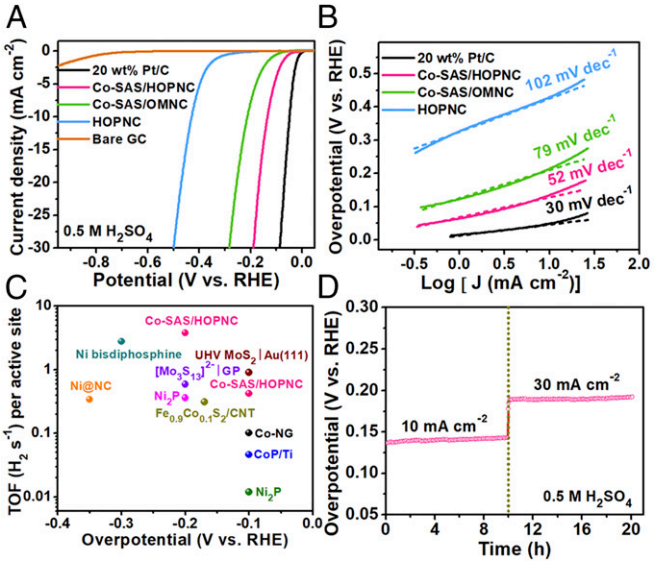

Fig. 4. Electrocatalytic performance evaluation of catalysts for HER in 0.5 M H_2SO_4. (*A*) HER polarization curves for the Co-SAS/HOPNC, Co-SAS/OMNC, HOPNC, bare glassy carbon (GC) electrode, and 20 wt % Pt/C. (*B*) Tafel plots derived from *A*. (*C*) TOF values of Co-SAS/HOPNC in comparison with other representative catalysts. (*D*) Time-dependent catalytic overpotential curve of the Co-SAS/HOPNC at current density of 10 and then 30 mA cm^{-2} for 20 h.

Fig. 3*C*, the lowest Tafel slope of Co-SAS/HOPNC (58 mV dec^{-1}) among all of the studied catalysts further verified a faster kinetics.

The fuel cross-over effect resulting from methanol was evaluated via chronoamperometric tests. After the injection of 3 M methanol into the electrolyte of O_2-saturated 0.1 M KOH, Pt/C catalyst presents a sharp decline in the current density, whereas no obvious activity attenuation can be observed for Co-SAS/HOPNC (*SI Appendix*, Fig. S11), demonstrating that the Co-SAS/HOPNC catalyst possesses an excellent tolerance to methanol cross-over effect. Moreover, the durability of Co-SAS/HOPNC was also assessed by the accelerated durability tests (ADT) conducted by electrode cycling between 0.5 and 1.0 V with a sweep rate of 100 mV s^{-1} (Fig. 3*D*) in 0.1 M KOH saturated with O_2. After 5,000 potential cycles, little negative shift in $E_{1/2}$ (~3 mV) was shown on Co-SAS/HOPNC, in contrast to a larger $E_{1/2}$ shift of Pt/C (~26 mV) (*SI Appendix*, Fig. S12), confirming a remarkable catalytic durability of Co-SAS/HOPNC. AC HAADF-STEM (*SI Appendix*, Fig. S13) reveals that the single-atomic metal sites are still well distributed after durability test, which further verified the high stability of the Co-SAS/HOPNC.

Electrocatalytic Performance Evaluation for HER. Apart from ORR, the electrocatalytic HER performance of the Co-SAS/HOPNC was also investigated in acidic electrolyte (Ar-saturated 0.5 M H_2SO_4). The corresponding polarization curves of the studied samples are shown in Fig. 4*A*. The Co-SAS/HOPNC requires an overpotential of merely 137 mV to drive a current density of 10 mA cm^{-2}, which is much smaller than that of the Co-SAS/OMNC (214 mV) and HOPNC (427 mV). It also displays a good HER catalytic activity in alkaline solution (*SI Appendix*, Fig. S14). Moreover, the Co-SAS/HOPNC shows a Tafel slope of 52 mV dec^{-1}, indicating a higher activity than that of Co-SAS/OMNC (79 mV dec^{-1}) and HOPNC (102 mV dec^{-1}) (Fig. 4*B*). The HER activity of Co-SAS/HOPNC is better than those observed for the majority of non–precious-metal HER electrocatalysts in acidic medium (*SI Appendix*, Table S4). The exchange current density (J_0) of the Co-SAS/HOPNC was determined to be 0.105 mA cm^{-2}, significantly larger than that of the other studied nonprecious samples (*SI Appendix*, Fig. S15). Electrochemical impedance spectroscopy (EIS) investigations were conducted to offer further insight into the electrode kinetics of the electrocatalysts. The Nyquist plots of the Co-SAS/HOPNC, Co-SAS/OMNC, and HOPNC are exhibited in *SI Appendix*, Fig. S16. A simplified equivalent circuit model that consists of series resistance (R_s), constant phase element (CPE1, CPE2), and charge-transfer resistance (R_{ct}) was used to fit the EIS data. It is well accepted that the width of the semicircle at high-frequency regions corresponds to the R_{ct} and reflects the overall electrochemical kinetics (33). Importantly, the Co-SAS/HOPNC has much smaller R_{ct} value of 46.2 Ω than that of Co-SAS/OMNC and HOPNC, confirming a faster reaction kinetics on Co-SAS/HOPNC. These results confirm the crucial role of the isolated metal-N coordination sites and the importance of unique hierarchically ordered porous structure in catalyzing the generation of H_2 (34–37).

The TOF values of the Co-SAS/HOPNC in 0.5 M H_2SO_4 were calculated to be 0.41 and 3.8 s^{-1} at an overpotential of 100 and 200 mV, respectively (for calculation details, see *SI Appendix*). These values are superior to those of recently reported scalable HER electrocatalysts based on non-precious-metal materials (Fig. 4*C* and *SI Appendix*, Table S5). To assess the durability of the Co-SAS/HOPNC catalyst for HER in acidic medium, the ADT were conducted by potential cycling between −0.3 and 0.2 V at a scanning rate of 100 mV s^{-1} in Ar-saturated 0.5 M H_2SO_4. As presented in *SI Appendix*, Fig. S17, we can see that the Co-SAS/HOPNC exhibits negligible activity loss after 2,000 continuous potential cycles. In contrast, the polarization curve of Pt/C shifts cathodically by more than 28 mV at a current density of 30 mA cm^{-2} upon cycling. This proves the greater stability of Co-SAS/HOPNC compared with that of Pt/C. In addition, the long-term durability of the Co-SAS/HOPNC was also evaluated consecutively at current densities of 10 and 30 mA cm^{-2} (Fig. 4*D*). The catalytic overpotential shows no appreciable increase after 20 h continuous operation. These results confirm the superior durability of the Co-SAS/HOPNC catalyst in the long-term electrochemical process.

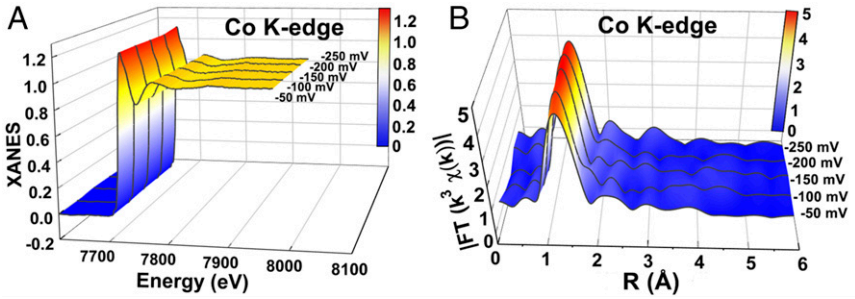

Fig. 5. In situ XAS experiments. In situ XANES spectra (*A*) and FT- EXAFS spectra (*B*) at Co *K* edge of Co-SAS/HOPNC at different potentials.

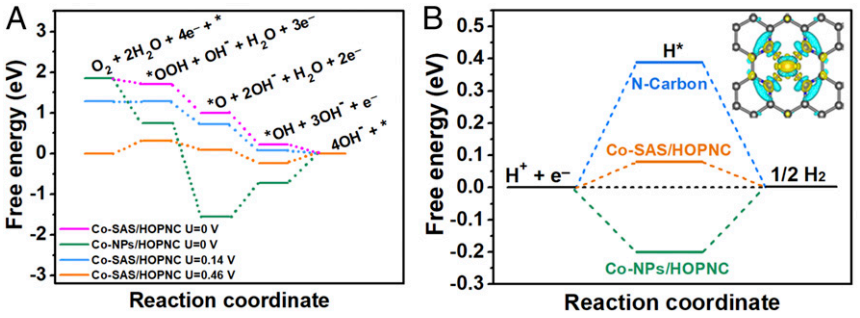

Fig. 6. DFT calculations. (*A*) Calculated free-energy diagram of ORR on Co-SAS/HOPNC and Co-NPs/HOPNC in alkaline media. (*B*) Calculated free-energy diagram of HER on Co-SAS/HOPNC, Co-NPs/HOPNC, and *N*-graphene. (*Inset*) The charge-density distribution image of Co-SAS/HOPNC, implying that the Co single atoms are positively charged via the charge transfer from Co to N.

The in situ X-ray absorption spectroscopy (XAS) measurements for Co-SAS/HOPNC were performed in 0.5 M H_2SO_4 to directly monitor the atomic structures of the single Co sites as well as their coordination environment under HER electrocatalytic conditions and the data were recorded on a setup equipped with a solid-state detector (*SI Appendix*, Fig. S18). The XAFS curves of the Co *K* edge were collected at different potentials. The Co-SAS/HOPNC retains stable local atomic structure during the catalytic H_2 evolution process with no obvious changes in the in situ Co *K*-edge XANES spectra (Fig. 5*A*) and the corresponding EXAFS spectra (Fig. 5*B*). The SEM, TEM, EDS maps, AC HAADF-STEM, and XAFS characterizations (*SI Appendix*, Figs. S19–S22) further show that the atomically distributed Co sites and the ordered interconnected macro- and mesoporous structure are well maintained after the ADT test.

ORR and HER Enhancement Mechanism. To confirm that isolated Co-N_4 coordination sites contribute to the electrocatalytic ORR and HER, the Co nanoparticles (NPs)-/HOPNC sample was prepared for comparative study. Some Co-based NPs on the ordered porous carbon are observed in the TEM images of Co-NPs/HOPNC (*SI Appendix*, Fig. S23). After leaching the Co-NPs/HOPNC sample in 0.5 M H_2SO_4 at 90 °C for 24 h, the cobalt-based NPs were removed and the isolated cobalt sites retained (*SI Appendix*, Figs. S24–S26). The acid-leached Co-NPs/HOPNC catalyst exhibits a significantly increased $E_{1/2}$ for ORR (*SI Appendix*, Fig. S27*A*) and an apparent larger reduction current for HER compared with the Co-NPs/HOPNC (*SI Appendix*, Fig. S27*B*), suggesting that the enhanced ORR and HER activities of the Co-SAS/HOPNC catalyst originates from the isolated Co-N_4 coordination sites.

The DFT calculations were carried out to obtain a deep understanding of the excellent electrocatalytic activity of Co-SAS/HOPNC catalyst. The computational details are provided in *SI Appendix*, Figs. S28 and S29 and Tables S6–S8. We obtained free-energy diagrams along reaction coordinate based on Nørskov et al.'s (38) computational hydrogen electrode model. The calculated free-energy diagrams for $4e^-$ reduction pathway of ORR over Co-SAS/HOPNC and Co particles in alkaline media (pH = 13) are shown in Fig. 6*A*. All ORR steps over Co-SAS/HOPNC are exothermic (downhill in free energy) at zero potential, indicating a facile reaction. For ORR over Co-NPs/HOPNC at U = 0 V, the steps of *O to *OH and *OH to OH^- are endothermic by 0.83 and 0.73 eV, respectively. Thus, the comparison of free-energy profiles demonstrates that the ORR activity of Co-SAS/HOPNC is superior to that of Co-NPs/HOPNC, which benefits from the presence of the isolated Co-N_4 coordination sites. As the potential increases to 0.14 V, formation of *OOH over Co-SAS/HOPNC becomes uphill in free energy. At the equilibrium potential (U = 0.46 V) for the overall $4e^-$ reduction of ORR over Co-SAS/HOPNC, steps of formation of *OOH and OH^- are endothermic. For the HER, it has been proven that Gibbs free energy of hydrogen adsorption (ΔG_{H^*}) is a major descriptor of HER catalytic activity, and the optimal ΔG_{H^*} is around 0 eV (39–41). The ΔG_{H^*} values of Co-SAS/HOPNC along with Co particles and *N*-doped graphene for comparison were investigated. The negative ΔG_{H^*} (−0.20 eV) value of Co particles indicates a relatively strong hydrogen adsorption on its surface, while the positive ΔG_{H^*} value of 0.39 eV for *N*-doped graphene reveals a very weak H* adsorption, which both are disadvantageous to HER (Fig. 6*B*). Significantly, for the Co-SAS/HOPNC catalyst, the ΔG_{H^*} value can be significantly reduced to

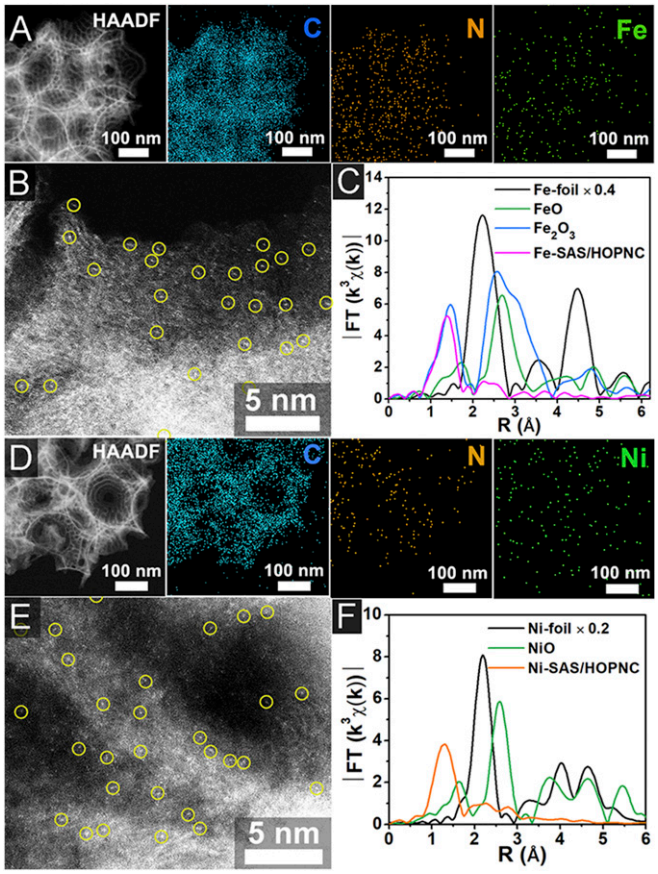

Fig. 7. Characterization of Fe-SAS/HOPNC and Ni-SAS/HOPNC. HAADF-STEM image and corresponding EDS maps of Fe-SAS/HOPNC (*A*) and Ni-SAS/HOPNC (*D*). AC HAADF-STEM images of Fe-SAS/HOPNC (*B*) and Ni-SAS/HOPNC (*E*). Isolated single atoms are marked in light-yellow circles. (*C*) FT at the Fe *K* edge of Fe-SAS/HOPNC, FeO, Fe_2O_3, and Fe foil samples. (*F*) FT at the Ni *K* edge of Ni-SAS/HOPNC, NiO, and Ni foil sample.

0.08 eV, in good agreement with the excellent catalytic activity of Co-SAS/HOPNC with the most favorable hydrogen adsorption–desorption property. Therefore, the superior HER activity of Co-SAS/HOPNC in acidic solution can be derived from the dramatically boosting of each reaction on single Co-N_4 site, which not only promote H adsorption but also facilitate H–H coupling.

Moreover, the present synthetic approach can be extended to prepare other M-SAS/HOPNC (M = Fe, Ni, etc.) materials (preparation details are presented in *SI Appendix*). The EDS maps (Fig. 7 *A* and *D*) and AC HAADF-STEM images (Fig. 7 *B* and *E*) of Fe-SAS/HOPNC and Ni-SAS/HOPNC demonstrate the atomic dispersion of Fe and Ni atoms on the HOPNC. The TEM images (*SI Appendix*, Fig. S30), X-ray diffraction (*SI Appendix*, Fig. S31), and XAFS curves (Fig. 7 *C* and *F* and *SI Appendix*, Figs. S32–S35 and Tables S9 and S10) also illustrate the single-atom form of Fe and Ni species. These results verify the generality of the synthetic method.

Conclusions

In summary, by using a dual-template cooperative pyrolysis strategy, we have prepared a series of M-SAS/HOPNC, M = Co, Fe, Ni, etc.). Because of the synergetic effect of the atomically dispersed single Co sites and the unique hierarchical structure with ordered interconnected macropores and mesopores, the Co-SAS/HOPNC exhibits a remarkable bifunctional electrocatalytic activity for ORR and HER and long-term durability. Control experiments and DFT calculation results have confirmed the crucial role of isolated single Co sites to the catalytic activity. The distinct properties of the Co-SAS/HOPNC make it a promising substitute for Pt-based ORR and HER electrocatalysts. Additionally, this work provides an important route for developing families of efficient single-atomic-site catalysts with technological importance in various fields.

Methods

Details on the synthesis of Co-SAS/HOPNC catalyst, structure and electrochemical characterization, DFT calculation details, and in situ XAS measurements are provided in *SI Appendix*.

ACKNOWLEDGMENTS. We thank the BL14W1 in Shanghai Synchrotron Radiation Facility (SSRF) for XAS measurements. This work was supported by China Ministry of Science and Technology under Contract 2016YFA (0202801), the National Natural Science Foundation of China (Grants 21471089, 21671117, 21521091, 21390393, U1463202, and 21676018), and the China Postdoctoral Science Foundation (Grant 2017M610864).

1. Shi Y, Zhang B (2016) Recent advances in transition metal phosphide nanomaterials: Synthesis and applications in hydrogen evolution reaction. *Chem Soc Rev* 45: 1529–1541.
2. Wang R, Dong XY, Du J, Zhao JY, Zang SQ (2018) MOF-derived bifunctional Cu_3P nanoparticles coated by a N,P-codoped carbon shell for hydrogen evolution and oxygen reduction. *Adv Mater* 30:1703711.
3. Shui J, Chen C, Grabstanowicz L, Zhao D, Liu DJ (2015) Highly efficient nonprecious metal catalyst prepared with metal-organic framework in a continuous carbon nanofibrous network. *Proc Natl Acad Sci USA* 112:10629–10634.
4. Zheng Y, et al. (2017) Molecule-level g-C_3N_4 coordinated transition metals as a new class of electrocatalysts for oxygen electrode reactions. *J Am Chem Soc* 139: 3336–3339.
5. Lu SQ, Zhuang ZB (2016) Electrocatalysts for hydrogen oxidation and evolution reactions. *Sci China Mater* 59:217–238.
6. Zhang J, et al. (2016) N,P-codoped carbon networks as efficient metal-free bifunctional catalysts for oxygen reduction and hydrogen evolution reactions. *Angew Chem Int Ed Engl* 55:2230–2234.
7. Liu S, et al. (2017) Metal-organic-framework-derived hybrid carbon nanocages as a bifunctional electrocatalyst for oxygen reduction and evolution. *Adv Mater* 29: 1700874.
8. Fan L, et al. (2016) Atomically isolated nickel species anchored on graphitized carbon for efficient hydrogen evolution electrocatalysis. *Nat Commun* 7:10667.
9. Zou X, Zhang Y (2015) Noble metal-free hydrogen evolution catalysts for water splitting. *Chem Soc Rev* 44:5148–5180.
10. Wang J, et al. (2017) A Co-N/C hollow-sphere electrocatalyst derived from a metanilic CoAl layered double hydroxide for the oxygen reduction reaction, and its active sites in various pH media. *Nano Res* 10:2508–2518.
11. Wang H, et al. (2013) Electrochemical tuning of vertically aligned MoS_2 nanofilms and its application in improving hydrogen evolution reaction. *Proc Natl Acad Sci USA* 110: 19701–19706.
12. Jia Y, et al. (2017) A heterostructure coupling of exfoliated Ni–Fe hydroxide nanosheet and defective graphene as a bifunctional electrocatalyst for overall water splitting. *Adv Mater* 29:1700017.
13. Long B, Tang Y, Li J (2016) New mechanistic pathways for CO oxidation catalyzed by single-atom catalysts: Supported and doped Au_1/ThO_2. *Nano Res* 9:3868–3880.
14. Yang HC, et al. (2017) Atomic-scale Pt clusters decorated on porous α-$Ni(OH)_2$ nanowires as highly efficient electrocatalyst for hydrogen evolution reaction. *Sci China Mater* 60:1121–1128.
15. Qiao B, et al. (2011) Single-atom catalysis of CO oxidation using Pt_1/FeO_x. *Nat Chem* 3: 634–641.
16. Chen YJ, et al. (2018) Single-atom catalysts: Synthetic strategies and electrochemical applications. *Joule* 2:1242–1264.
17. Zhu C, Fu S, Shi Q, Du D, Lin Y (2017) Single-atom electrocatalysts. *Angew Chem Int Ed Engl* 56:13944–13960.
18. Gao G, Jiao Y, Waclawik ER, Du A (2016) Single atom (Pd/Pt) supported on graphitic carbon nitride as an efficient photocatalyst for visible-light reduction of carbon dioxide. *J Am Chem Soc* 138:6292–6297.
19. Zhang C, et al. (2017) Single-atomic ruthenium catalytic sites on nitrogen-doped graphene for oxygen reduction reaction in acidic medium. *ACS Nano* 11:6930–6941.
20. Li F, et al. (2015) Atomic mechanism of electrocatalytically active Co-N complexes in graphene basal plane for oxygen reduction reaction. *ACS Appl Mater Interfaces* 7: 27405–27413.
21. Zitolo A, et al. (2015) Identification of catalytic sites for oxygen reduction in iron- and nitrogen-doped graphene materials. *Nat Mater* 14:937–942.
22. Zitolo A, et al. (2017) Identification of catalytic sites in cobalt-nitrogen-carbon materials for the oxygen reduction reaction. *Nat Commun* 8:957.
23. Fei HL, et al. (2018) General synthesis and definitive structural identification of MN_4C_4 single-atom catalysts with tunable electrocatalytic activities. *Nat Catal* 1:63–72.
24. Liang HW, Wei W, Wu ZS, Feng X, Müllen K (2013) Mesoporous metal-nitrogen-doped carbon electrocatalysts for highly efficient oxygen reduction reaction. *J Am Chem Soc* 135:16002–16005.
25. Yuan ZY, Su BL (2006) Insights into hierarchically meso–macroporous structured materials. *J Mater Chem* 16:663–677.
26. Zhang J, Zhao Z, Xia Z, Dai L (2015) A metal-free bifunctional electrocatalyst for oxygen reduction and oxygen evolution reactions. *Nat Nanotechnol* 10:444–452.
27. Sun TT, et al. (2018) General synthesis of 3D ordered macro-/mesoporous materials by templating mesoporous silica confined in opals. *Chem Mater* 30:1617–1624.
28. Zhou H, et al. (2017) Highly active catalyst derived from a 3D foam of $Fe(PO_3)_2/Ni_2P$ for extremely efficient water oxidation. *Proc Natl Acad Sci USA* 114:5607–5611.
29. Zhu QL, et al. (2017) Atomically dispersed Fe/N-doped hierarchical carbon architectures derived from a metal-organic framework composite for extremely efficient electrocatalysis. *ACS Energy Lett* 2:504–511.
30. Deng J, et al. (2017) Multiscale structural and electronic control of molybdenum disulfide foam for highly efficient hydrogen production. *Nat Commun* 8:14430.
31. Cho HJ, Kim D, Li J, Su D, Xu B (2018) Zeolite-encapsulated Pt nanoparticles for tandem catalysis. *J Am Chem Soc* 140:13514–13520.
32. Yin P, et al. (2016) Single cobalt atoms with precise N-coordination as superior oxygen reduction reaction catalysts. *Angew Chem Int Ed Engl* 55:10800–10805.
33. Wu Y, et al. (2018) Electron density modulation of $NiCo_2S_4$ nanowires by nitrogen incorporation for highly efficient hydrogen evolution catalysis. *Nat Commun* 9:1425.
34. Ma TY, Dai S, Jaroniec M, Qiao SZ (2014) Metal-organic framework derived hybrid Co_3O_4-carbon porous nanowire arrays as reversible oxygen evolution electrodes. *J Am Chem Soc* 136:13925–13931.
35. Liang J, Du X, Gibson C, Du XW, Qiao SZ (2013) N-doped graphene natively grown on hierarchical ordered porous carbon for enhanced oxygen reduction. *Adv Mater* 25: 6226–6231.
36. Sun TT, et al. (2016) Ordered mesoporous nickel sphere arrays for highly efficient electrocatalytic water oxidation. *ACS Catal* 6:1446–1450.
37. Lai JP, Nsabimana A, Luque R, Xu GB (2018) 3D porous carbonaceous electrodes for electrocatalytic applications. *Joule* 2:76–93.
38. Nørskov JK, et al. (2004) Origin of the overpotential for oxygen reduction at a fuel-cell cathode. *J Phys Chem B* 108:17886–17892.
39. Hinnemann B, et al. (2005) Biomimetic hydrogen evolution: MoS_2 nanoparticles as catalyst for hydrogen evolution. *J Am Chem Soc* 127:5308–5309.
40. Skúlason E, et al. (2010) Modeling the electrochemical hydrogen oxidation and evolution reactions on the basis of density functional theory calculations. *J Phys Chem C* 114:18182–18197.
41. Duan H, et al. (2017) High-performance Rh_2P electrocatalyst for efficient water splitting. *J Am Chem Soc* 139:5494–5502.